1D finite element artificial boundary method for layered half space site response from obliquely incident earthquake

Mi Zhao[*1], Houquan Yin[1], Xiuli Du[1], Jingbo Liu[2] and Lingyu Liang[1]

[1]*The Key Laboratory of Urban Security and Disaster Engineering of Ministry of Education,
Beijing University of Technology, Beijing 100124, China*
[2]*Department of Civil Engineering, Tsinghua University, Beijing 100084, China*

Abstract. Site response analysis is an important topic in earthquake engineering. A time-domain numerical method called as one-dimensional (1D) finite element artificial boundary method is proposed to simulate the homogeneous plane elastic wave propagation in a layered half space subjected to the obliquely incident plane body wave. In this method, an exact artificial boundary condition combining the absorbing boundary condition with the inputting boundary condition is developed to model the wave absorption and input effects of the truncated half space under layer system. The spatially two-dimensional (2D) problem consisting of the layer system with the artificial boundary condition is transformed equivalently into a 1D one along the vertical direction according to Snell's law. The resulting 1D problem is solved by the finite element method with a new explicit time integration algorithm. The 1D finite element artificial boundary method is verified by analyzing two engineering sites in time domain and by comparing with the frequency-domain transfer matrix method with fast Fourier transform.

Keywords: seismic site response analysis; layered half space; oblique incidence; Snell's law; finite element method; artificial boundary condition

1. Introduction

Seismic response analysis of engineering site is an important topic in earthquake engineering. The practical site is usually simplified as the horizontally layered soil deposits resting on the half space bedrock. This can be called as the layered half space model. The earthquake wave propagates from the half space bedrock into the layered soil deposits. The incident wave is assumed as the plane body wave due to the site far from the earthquake source. The methods to calculate the layered half space site responses have been developed in the past several decades. They will be reviewed simply as follows.

When the seismic wave is incident vertically for the deep focus earthquake, the site response analysis is a spatially one-dimensional (1D) problem in nature. The methods and corresponding computer programs for the 1D site response analysis have been developed, even to consider the

∗Corresponding author, Professor, E-mail: zhaomi@bjut.edu.cn

nonlinear soil behavior. They can be seen in the review on recent advances (Hashash *et al.* 2010) and the applications (Rota *et al.* 2011, Mayoral *et al.* 2011). On the other hand, for a shallow focus earthquake and when the engineering site moderately far from the epicenter, the oblique incidence of the seismic wave should be considered. The problem is thus spatially two-dimensional (2D) in nature, leading to the site response analysis method more complex than that for the 1D case. The vertical incidence of the seismic wave is actually a special case of the oblique incidence.

The transfer matrix method (Thomson 1950, Haskell 1953, Knopoff 1964, Dunkin 1965, Gilbert and Backus 1966, Watson 1970) and the stiffness matrix method (Kausel and Roësset 1981, Kausel 2006, Wolf and Obernhuber 1982a, b, 1983, Takano *et al.* 1988) can be used to solve the 2D site response problem subjected to the obliquely incident seismic wave, although they can consider the general load source besides the obliquely incident plane wave studied here. The two methods belong to the analytical method in frequency domain. They are therefore used to calculate the elastic site response at present. To consider the nonlinear soil behavior using the constitutive relation, the numerical method in time domain is required.

The thin layer method (Lysmer 1970, Lysmer and Waas 1972, Kausel and Peek 1982, Kausel 2000, 2004, Park and Kausel 2004, Jones and Hunt 2011) is a discretization edition of the stiffness matrix method along the depth. It is developed originally in frequency domain and regards the underlying half space as rigid bedrock. The time-domain formulation of the thin layer method for the layer system has been given by Kausel (1994). The radiation damping (wave absorption effect) of the elastic underlying half space is simulated by the absorbing (also called as radiation, nonreflecting, or transmitting) boundary condition such as the early second-order paraxial boundary (Seale and Kausel 1984, 1989) and the recent perfectly matched layer (Barbosa *et al.* 2012). However, these absorbing boundary conditions are approximate for the 2D site response problem to simulate the plane wave propagation in the layered half space.

Several time-domain numerical methods for 2D site response problem have also been developed in recent years. Liao *et al.* (1994) study the SH wave propagation case where the elasto-plastic multi-yield surface constitutive model with a kinematic hardening rule is used to consider the nonlinear hysteretic behavior of soil under the irregular cyclic loading. In their work the wave absorption effect of the truncated underlying half space is modeled exactly by the well-known viscous absorbing boundary condition (Lysmer and Kuhlemeyer 1969). The 2D problem of spatially infinite along the layer direction (horizontal direction) is transformed into a 1D one based on Snell's law. The finite difference method along the characteristic lines is used to solve the resulting 1D problem. However, the P-SV wave propagation case that is more complex than the SH wave case has not been studied.

The fourth author and his coworker (Liu and Wang 2006, 2007) study the SH and P-SV wave propagation cases but only consider the linearly elastic soil. In their work the viscous absorbing boundary condition is still used to model the wave absorption effect of the truncated half space. This is an approximate treatment to the P-SV wave case, leading to the responses with low accuracy. The finite element method with the central difference time integration algorithm is applied directly to the 2D problem of spatially infinite along the layer direction. Snell's law is then used to transform the 2D discrete problem into the spatially 1D one. However, this method has a stability limitation on the time step size of integration although it has an implicit time integration form of solving the linear equation system. Moreover, the numerical dispersive error of this method is consistent with that of 2D finite element method instead of with that of 1D one.

According to the state of art on the time-domain numerical methods mentioned above, a good framework of the computational method for the 2D site response problem due to the obliquely

incident earthquake wave, even for the elastic wave case, is not yet seen by the authors. In this paper, a time-domain numerical method called as 1D finite element artificial boundary method is proposed for the layered half space site response analysis subjected to the obliquely incident plane body wave. Only the linearly elastic case is studied in the present paper, while the extension to the nonlinear case in further. The remainder of this paper is organized as follows. The problem is stated in Section 2. An exact artificial boundary condition is proposed in Section 3 to model the wave absorption and input effects of the truncated underlying half space. A 1D explicit finite element method is developed in Section 4 to solve the spatially infinite 2D layer system with the exact artificial boundary condition. The 1D finite element artificial boundary method is verified in Section 5 by analyzing two typical engineering sites and by comparing with the transfer matrix method with fast Fourier transform. Conclusions follow in Section 6.

2. Problem statement

According to the elastic wave theory, the plane wave propagation in a layered half space can be decomposed into two wave problems in 2D space, i.e., the P-SV wave and SH wave problems. This paper considers the P-SV wave problem of linear elasticity for which there is not yet a good time-domain numerical method so far. The 2D layered half space subjected to the obliquely incident plane P or SV wave is shown in Fig. 1. The Cartesian coordinate system is (x, z). The N-1 horizontal layers and the underlying half space are numbered from top to bottom as 1, 2, …, N in turn. The thicknesses of the layers from 1 to N-1 is h^1, h^2, …, h^{N-1} in turn. The ρ^j, c_P^j and c_S^j are the mass density, P wave velocity and S wave velocity, respectively, with the superscripts j=1,…,N-1 for the layers and j=N for the underlying half space. The incident angle θ of the plane body wave is defined as the angle between the wave propagation and vertical directions.

The strain-displacement relation is

$$\boldsymbol{\varepsilon}^j = \mathbf{L}\mathbf{u}^j \tag{1}$$

where $\mathbf{u}^j = \left\{ u_x^j \quad u_z^j \right\}^{\mathrm{T}}$ and $\boldsymbol{\varepsilon}^j = \left\{ \varepsilon_x^j \quad \varepsilon_z^j \quad \varepsilon_{xz}^j \right\}^{\mathrm{T}}$ are the displacement and strain vectors, respectively; the superscript T denotes the matrix transpose; and the differential operator matrix is

$$\mathbf{L} = \begin{bmatrix} \dfrac{\partial}{\partial x} & 0 & \dfrac{\partial}{\partial z} \\ 0 & \dfrac{\partial}{\partial z} & \dfrac{\partial}{\partial x} \end{bmatrix}^{\mathrm{T}} \tag{2}$$

The stress-strain relation is

$$\boldsymbol{\sigma}^j = \mathbf{D}^j \boldsymbol{\varepsilon}^j \tag{3}$$

where $\boldsymbol{\sigma}^j = \left\{ \sigma_x^j \quad \sigma_z^j \quad \tau_{xz}^j \right\}^{\mathrm{T}}$ is the stress vector; and the constitutive matrix of linear elasticity can be written as

$$\mathbf{D}^j = \rho^j (c_P^j)^2 \begin{bmatrix} 1 & 1 & 0 \\ 1 & 1 & 0 \\ 0 & 0 & 0 \end{bmatrix} + \rho^j (c_S^j)^2 \begin{bmatrix} 0 & -2 & 0 \\ -2 & 0 & 0 \\ 0 & 0 & 1 \end{bmatrix} \tag{4}$$
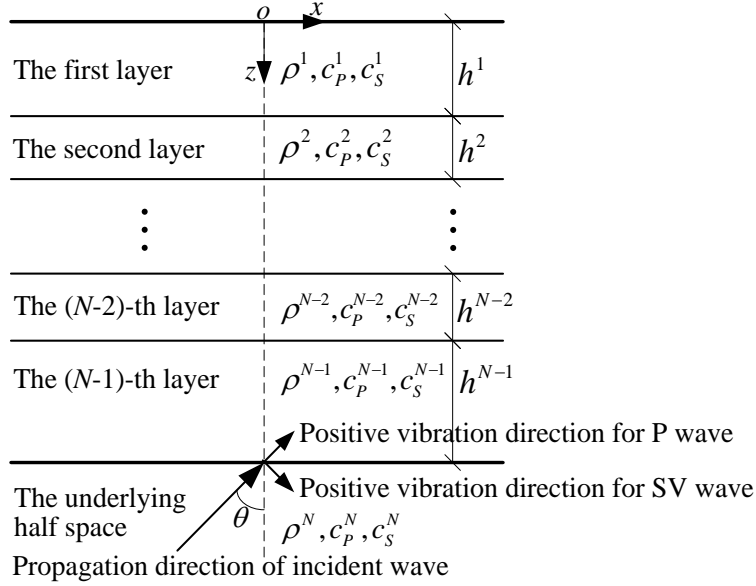
Fig. 1 The layered half space subjected to the obliquely incident plane body wave

The dynamic equilibrium equation is

$$\mathbf{L}^{\mathrm{T}}\boldsymbol{\sigma}^j = \rho^j \ddot{\mathbf{u}}^j \tag{5}$$

where the dot over the variable denotes the derivative to time t. Substituting Eq. (1) into Eq. (3) and then the result into Eq. (5) obtain the elastic dynamic equation represented by the displacements as

$$\mathbf{L}^{\mathrm{T}}\mathbf{D}^j\mathbf{L}\mathbf{u}^j = \rho^j \ddot{\mathbf{u}}^j \tag{6}$$

Define the stress vector on the surface of constant z as $\boldsymbol{\sigma}_z^j = \left\{ \tau_{xz}^j \quad \sigma_z^j \right\}^{\mathrm{T}}$. The boundary condition on the free surface is

$$\boldsymbol{\sigma}_z^1 = \mathbf{0} \tag{7}$$

The boundary conditions at the interfaces between any two adjacent layers and between the lowest layer and underlying half space are the continuity conditions of the displacements and stresses. They can be written as

$$\mathbf{u}^j = \mathbf{u}^{j+1} \tag{8}$$

$$\boldsymbol{\sigma}_z^j = \boldsymbol{\sigma}_z^{j+1} \tag{9}$$

The plane P or SV wave is obliquely incident from the underlying half space into the layer system. At the initial instant of time $t=0$, the wavefront of the incident wave passes through the intersection point of the z coordinate axis and the lowest interface (or the artificial boundary introduced later). The known displacement time history of the incident wave at this intersection

point is denoted as $u_{P0} = u_{P0}(t)$ for the P wave or $u_{S0} = u_{S0}(t)$ for the SV wave. The positive direction of this time history is shown in Fig. 1. Besides the incident wave, no load source or initial condition exists in the layered half space.

3. Exact artificial boundary condition

An artificial boundary is introduced along the lowest interface to truncate the underlying half space. Actually the artificial boundary can be set as a horizontal line at any location in the underlying half space. An exact artificial boundary condition combining the absorbing boundary condition with the inputting boundary condition is developed to model the wave absorption and input effects of the truncated half space.

3.1 Plane wave solution

The displacements in the underlying half space can be represented by the potential functions as

$$\mathbf{u}^N = \begin{bmatrix} \dfrac{\partial}{\partial x} & -\dfrac{\partial}{\partial z} \\ \dfrac{\partial}{\partial z} & \dfrac{\partial}{\partial x} \end{bmatrix} \boldsymbol{\varphi}^N \tag{10}$$

where $\boldsymbol{\varphi}^N = \left\{ \varphi_P^N \quad \varphi_S^N \right\}^T$ is the potential function vector with the subscripts P and S respectively for P and SV waves. The homogeneous plane wave solutions can be divided into two parts as

$$\boldsymbol{\varphi}^N = \overline{\boldsymbol{\varphi}}^N + \hat{\boldsymbol{\varphi}}^N \tag{11}$$

The unknown scattered waves are

$$\overline{\boldsymbol{\varphi}}^N = \begin{Bmatrix} \overline{f}_P \left(m_P x + n_P z - c_P^N t \right) \\ \overline{f}_S \left(m_S x + n_S z - c_S^N t \right) \end{Bmatrix} \tag{12}$$

The known incident P or SV wave, respectively, is

$$\hat{\boldsymbol{\varphi}}^N = \begin{Bmatrix} \hat{f}_P \left(m_P x - n_P z - c_P^N t \right) \\ 0 \end{Bmatrix} \tag{13}$$

$$\hat{\boldsymbol{\varphi}}^N = \begin{Bmatrix} 0 \\ \hat{f}_S \left(m_S x - n_S z - c_S^N t \right) \end{Bmatrix} \tag{14}$$

In Eqs. (12)-(14), $\overline{f}_P$, $\overline{f}_S$, $\hat{f}_P$ and $\hat{f}_S$ are the wave functions; and m_P, n_P, m_S and n_S are

$$m_P = \frac{c_P^N}{c_x}, \quad n_P = \sqrt{1 - \left(\frac{c_P^N}{c_x} \right)^2}, \quad m_S = \frac{c_S^N}{c_x} \text{ and } n_S = \sqrt{1 - \left(\frac{c_S^N}{c_x} \right)^2} \tag{15}$$

where c_x is the apparent velocity of the plane waves propagating along the x direction, which satisfies

$$c_x = \begin{cases} \dfrac{c_P^N}{\sin\theta} & \text{for P wave incidence} \\[2mm] \dfrac{c_S^N}{\sin\theta} & \text{for SV wave incidence} \end{cases} \tag{16}$$

Corresponding to the potential function decomposition of Eq. (11), the velocities and stresses can also be divided into the scattered wave and incident wave parts as

$$\dot{\mathbf{u}}^N = \bar{\dot{\mathbf{u}}}^N + \hat{\dot{\mathbf{u}}}^N \tag{17}$$

$$\boldsymbol{\sigma}_z^N = \bar{\boldsymbol{\sigma}}_z^N + \hat{\boldsymbol{\sigma}}_z^N \tag{18}$$

3.2 Absorbing boundary condition

For the scattered waves, substituting Eq. (12) into Eq. (10) and then differentiating the result to time obtain the velocities as

$$\bar{\dot{\mathbf{u}}}^N = -c_x \begin{bmatrix} m_P^2 & -m_S n_S \\ m_P n_P & m_S^2 \end{bmatrix} (\bar{\boldsymbol{\varphi}}^N)'' \tag{19}$$

where the prime denotes the derivative of the function.

Substituting Eq. (12) into Eq. (10), then the result into Eq. (1) and finally the result into Eq. (3) obtain the stresses as

$$\bar{\boldsymbol{\sigma}}_z^N = \rho^N c_x^2 \begin{bmatrix} 2m_P n_P m_S^2 & m_S^2(2m_S^2 - 1) \\ m_P^2(1 - 2m_S^2) & 2m_S^3 n_S \end{bmatrix} (\bar{\boldsymbol{\varphi}}^N)'' \tag{20}$$

By combining Eq. (19) with Eq. (20) to eliminate the potential functions, the stress-velocity relation for the scattered waves can be obtained as

$$\bar{\boldsymbol{\sigma}}_z^N = -\mathbf{S}\bar{\dot{\mathbf{u}}}^N \tag{21}$$

with the impedance matrix

$$\mathbf{S} = \frac{\rho^N c_S^N}{m_P m_S + n_P n_S} \begin{bmatrix} n_P & 2n_P m_S n_S - m_P(1 - 2m_S^2) \\ m_P(1 - 2m_S^2) - 2n_P m_S n_S & m_P n_S / m_S \end{bmatrix} \tag{22}$$

Eq. (21) is an exact absorbing boundary condition at the artificial boundary of the layer system to model the wave absorption effect of the truncated half space. It can absorb the scattered waves propagating from the layer system into the half space without any wave reflection.

It can be proved that for the plane wave propagation case the stress-velocity relation Eq. (21) with the impedance matrix Eq. (22) is the time-domain form of the dynamic stiffness relation Eq. (9) with the half-space stiffness of Table 1 in the stiffness matrix method by Kausel and Roesset (1981).

3.3 Inputting boundary condition

For the incident P wave, substituting Eq. (13) into Eq. (10) and then differentiating the result to time obtain the velocities. Substituting Eq. (13) into Eq. (10), then the result into Eq. (1) and finally the result into Eq. (3) obtain the stresses. The resulting stresses and velocities lead to

$$\hat{\boldsymbol{\sigma}}_z^N = \mathbf{R}\dot{\hat{\mathbf{u}}}^N \tag{23}$$

with the impedance matrix

$$\mathbf{R} = \rho^N c_S^N \begin{Bmatrix} 2n_P m_S \\ m_P(2m_S^2 - 1)/m_S \end{Bmatrix} \{m_P \quad -n_P\} \tag{24}$$

For the incident SV wave, the stress-velocity relation with the same form as Eq. (23) can be obtained by carrying out the same manipulations as in the P wave incidence case. The impedance matrix for the incident SV wave can be written as

$$\mathbf{R} = \rho^N c_S^N \begin{Bmatrix} 1 - 2m_S^2 \\ 2m_S n_S \end{Bmatrix} \{n_S \quad m_S\} \tag{25}$$

Eq. (23) is an exact inputting boundary condition at the artificial boundary of the layer system to model the wave input effect of the truncated half space. It can input the known incident wave propagating from the half space into the layer system.

3.4 Artificial boundary condition

Substituting $\dot{\bar{\mathbf{u}}}^N = \dot{\mathbf{u}}^N - \dot{\hat{\mathbf{u}}}^N$ obtained from Eq. (17) into Eq. (21) and then substituting the result and Eq. (23) into Eq. (18) obtain

$$\boldsymbol{\sigma}_z^N = -\mathbf{S}\dot{\mathbf{u}}^N + (\mathbf{S} + \mathbf{R})\dot{\hat{\mathbf{u}}}^N \tag{26}$$

Eq. (26) is an exact artificial boundary condition combining the absorbing boundary condition for the scattered waves with the inputting boundary condition for the incident wave. By applying this stress-type exact artificial boundary condition to replace the truncated half space, the original spatially semi-infinite problem in the z direction is transformed equivalently into a spatially finite problem.

It can be proved that for the plane wave propagation case the layer system with boundary condition Eq. (26) is the time-domain form of the Eq. (12) with Eq. (19) or (20) in the stiffness matrix method by Kausel and Roesset (1981). However, the different reference systems are chosen in the two methods. Kausel and Roesset (1981) use a reference system that is a layer on the underlying half space or only the underlying half space, while this paper use a reference system that is a homogeneous full space. This equivalence has been explained in the Chapter 3 of the monographs by Wolf (1985).

4. 1D explicit finite element method

The spatially 2D problem that is defined by the layer system with the exact artificial boundary conditions is finite in the depth direction but infinite in the horizontal direction. It is transformed equivalently into a spatially 1D problem along the depth according to Snell's law. The resulting 1D problem is solved by the finite element method with a new explicit time integration algorithm. The high-accuracy stress computation method is presented.

4.1 Spatially 1D problem

According to Snell's law, all the plane waves propagating along the x direction in the layer system have the same apparent propagation velocity of Eq. (16). The differential operator relation can be obtained as

$$\frac{\partial}{\partial x} = -\frac{1}{c_x}\frac{\partial}{\partial t} \tag{27}$$

By applying Eq. (27) to Eq. (6) to eliminate the x-derivative, and after some manipulations, the control equation in the 1D space is obtained as

$$\mathbf{E}_1^j \frac{\partial^2 \mathbf{u}^j}{\partial z^2} - \mathbf{E}_2^j \frac{\partial \dot{\mathbf{u}}^j}{\partial z} = \mathbf{E}_3^j \ddot{\mathbf{u}}^j \tag{28}$$

with the coefficient matrices

$$\mathbf{E}_1^j = \rho^j \begin{bmatrix} (c_S^j)^2 & 0 \\ 0 & (c_P^j)^2 \end{bmatrix} \tag{29}$$

$$\mathbf{E}_2^j = \frac{\rho^j \left((c_P^j)^2 - (c_S^j)^2 \right)}{c_x} \begin{bmatrix} 0 & 1 \\ 1 & 0 \end{bmatrix} \tag{30}$$

$$\mathbf{E}_3^j = \rho^j \left(\mathbf{I}_2 - \frac{1}{c_x^2} \begin{bmatrix} (c_P^j)^2 & 0 \\ 0 & (c_S^j)^2 \end{bmatrix} \right) \tag{31}$$

where $\mathbf{I}_2$ is the two-order unit matrix.

Substituting Eq. (1) into Eq. (3) and then applying Eq. (27) to eliminate the x-derivative in the result obtain

$$\boldsymbol{\sigma}_z^j = \mathbf{E}_1^j \frac{\partial \mathbf{u}^j}{\partial z} - \mathbf{Q}^j \dot{\mathbf{u}}^j \tag{32}$$

with the coefficient matrix

$$\mathbf{Q}^j = \frac{\rho^j}{c_x} \begin{bmatrix} 0 & (c_S^j)^2 \\ (c_P^j)^2 - 2(c_S^j)^2 & 0 \end{bmatrix} \tag{33}$$

Substituting Eq. (32) into Eqs. (7)-(9) and Eq. (26), respectively, obtain the boundary condition on the free surface of the 1D problem

$$\mathbf{E}_1^1 \frac{\partial \mathbf{u}^1}{\partial z} = \mathbf{Q}^1 \dot{\mathbf{u}}^1 \tag{34}$$

the interface conditions of the 1D problem

$$\mathbf{u}^j = \mathbf{u}^{j+1} \quad \text{and} \quad (\mathbf{E}_1^{j+1} - \mathbf{E}_1^j)\frac{\partial \mathbf{u}^j}{\partial z} = (\mathbf{Q}^{j+1} - \mathbf{Q}^j)\dot{\mathbf{u}}^j \tag{35}$$

and the artificial boundary condition of the 1D problem

$$\mathbf{E}_1^{N-1} \frac{\partial \mathbf{u}^{N-1}}{\partial z} = -(\mathbf{S} - \mathbf{Q}^{N-1})\dot{\mathbf{u}}^{N-1} + (\mathbf{S} + \mathbf{R})\dot{\hat{\mathbf{u}}}^{N-1} \tag{36}$$

By setting $x=0$ the problem defined by Eq. (28) and Eqs. (34)-(36) is the spatially 1D one along the z coordinate axis. The zero initial condition (initially at rest) is given. At the artificial boundary point, the incident wave velocity vector can be given by the known velocity time history as

$$\dot{\hat{\mathbf{u}}}^{N-1} = \begin{cases} \{\sin\theta \quad -\cos\theta\}^{\mathrm{T}} \dot{u}_{P0} & \text{for P wave incidence} \\ \{\cos\theta \quad \sin\theta\}^{\mathrm{T}} \dot{u}_{S0} & \text{for SV wave incidence} \end{cases} \tag{37}$$

4.2 Explicit finite element method

The spatially 1D problem is discretized into a certain number of two-node finite elements. All elements and nodes, respectively, are numbered from top to bottom. For an element, the displacement can be interpolated as

$$\mathbf{u}^j = \mathbf{N}^e \mathbf{u}^e \tag{38}$$

where $\mathbf{N}^e$ is the interpolation function matrix; and $\mathbf{u}^e = \left\{\mathbf{u}_l^{\mathrm{T}} \quad \mathbf{u}_{l+1}^{\mathrm{T}}\right\}^{\mathrm{T}}$ is the nodal displacement vector of the element numbered as l. By applying the Galerkin finite element method with the linear interpolation function to the element controlled by Eq. (28), the dynamic equation can be obtained as

$$\mathbf{M}^e \ddot{\mathbf{u}}^e + \mathbf{C}^e \dot{\mathbf{u}}^e + \mathbf{K}^e \mathbf{u}^e = \mathbf{f}^e \tag{39}$$

with the element lumped mass matrix, the element damping matrix, the element stiffness matrix and the element loading vector, respectively, as

$$\mathbf{M}^e = \int_{z_l}^{z_{l+1}} \mathbf{N}^{e\mathrm{T}} \mathbf{E}_3^j \mathbf{N}^e \mathrm{d}z = \frac{\rho^j \Delta z}{2} \left(\mathbf{I}_4 - \frac{1}{c_x^2} \begin{bmatrix} (c_P^j)^2 & 0 & 0 & 0 \\ 0 & (c_S^j)^2 & 0 & 0 \\ 0 & 0 & (c_P^j)^2 & 0 \\ 0 & 0 & 0 & (c_S^j)^2 \end{bmatrix} \right) \tag{40}$$

$$\mathbf{C}^e = \int_{z_l}^{z_{l+1}} \mathbf{N}^{e\mathrm{T}} \mathbf{E}_2^j \frac{\partial \mathbf{N}^e}{\partial z} \mathrm{d}z = \frac{\rho^j \left((c_P^j)^2 - (c_S^j)^2 \right)}{2c_x} \begin{bmatrix} 0 & -1 & 0 & 1 \\ -1 & 0 & 1 & 0 \\ 0 & -1 & 0 & 1 \\ -1 & 0 & 1 & 0 \end{bmatrix} \tag{41}$$

$$\mathbf{K}^e = \int_{z_l}^{z_{l+1}} \frac{\partial \mathbf{N}^{e\mathrm{T}}}{\partial z} \mathbf{E}_1^j \frac{\partial \mathbf{N}^e}{\partial z} \mathrm{d}z = \frac{\rho^j}{\Delta z} \begin{bmatrix} (c_S^j)^2 & 0 & -(c_S^j)^2 & 0 \\ 0 & (c_P^j)^2 & 0 & -(c_P^j)^2 \\ -(c_S^j)^2 & 0 & (c_S^j)^2 & 0 \\ 0 & -(c_P^j)^2 & 0 & (c_P^j)^2 \end{bmatrix} \tag{42}$$

$$\mathbf{f}^e = \left\{ \begin{array}{c} -\mathbf{E}_1^j \left. \dfrac{\partial \mathbf{u}^j}{\partial z} \right|_{z=z_l} \\[2ex] \mathbf{E}_1^j \left. \dfrac{\partial \mathbf{u}^j}{\partial z} \right|_{z=z_{l+1}} \end{array} \right\} \tag{43}$$

where z_l is the nodal z coordinate; $\Delta z = z_{l+1} - z_l$ is the element length; and $\mathbf{I}_4$ is the four-order unit matrix. To solve the dynamic equation using the explicit time integration, the lumped mass matrix is used instead of the consistent one.

By assembling all finite elements and considering the boundary conditions Eqs. (34)-(36), the total dynamic equation for the spatially 1D problem is obtained as

$$\mathbf{M}\ddot{\mathbf{u}} + \mathbf{C}\dot{\mathbf{u}} + \mathbf{K}\mathbf{u} = \mathbf{f} \tag{44}$$

where $\mathbf{u} = \left\{ \mathbf{u}_1^{\mathrm{T}} \quad \mathbf{u}_2^{\mathrm{T}} \quad \cdots \quad \mathbf{u}_L^{\mathrm{T}} \right\}^{\mathrm{T}}$ is the total displacement vector of all L nodes; and the total mass matrix, the total damping matrix, the total stiffness matrix and the total loading vector, respectively, are

$$\mathbf{M} = \sum_e \mathbf{M}^e , \quad \mathbf{C} = \mathbf{C}_B + \sum_e \mathbf{C}^e \quad \text{and} \quad \mathbf{K} = \sum_e \mathbf{K}^e \tag{45}$$

Table 1 The constants for Leibstadt site in Switzeland

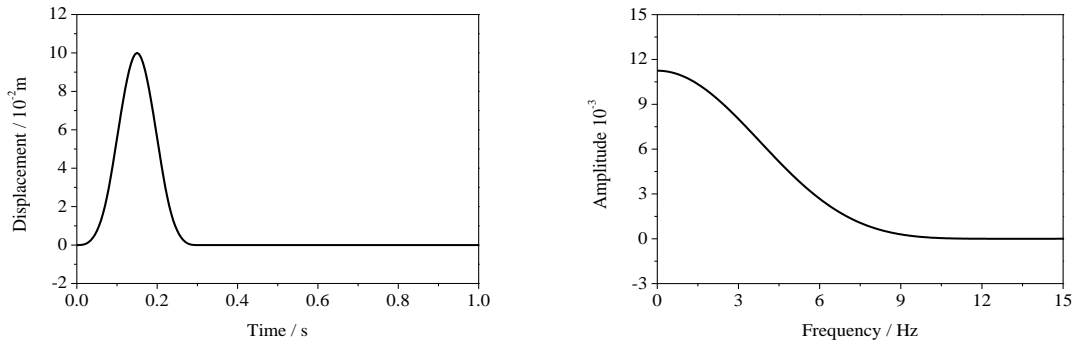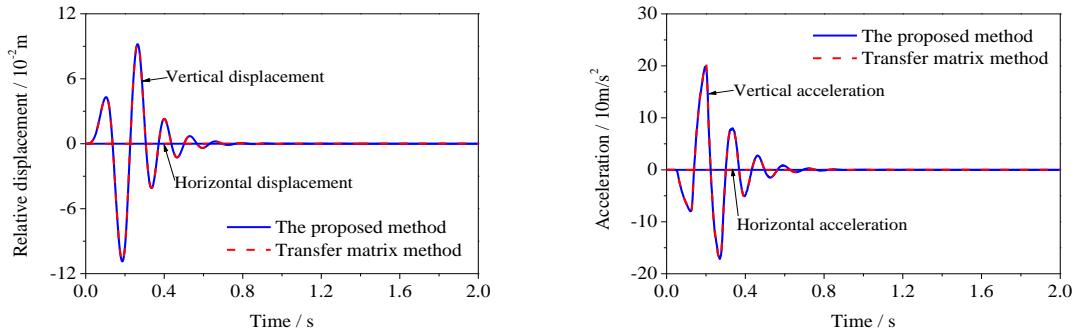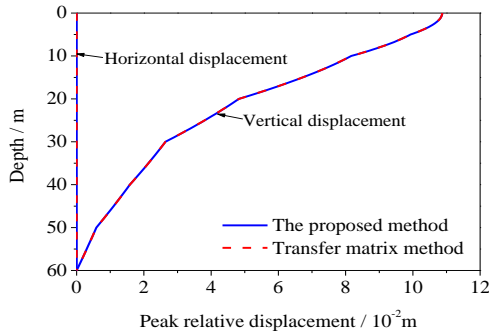| Layer thickness/m	Mass density/kg/m^3	P wave velocity/m/s	S wave velocity/m/s
5	2000	490	200
5	2000	612	250
10	2000	857	350
10	2200	1225	500
10	2200	1960	800
10	2400	2082	1000
∞	2500	2806	1500

Fig. 2 The displacement impulse and its frequency-spectrum amplitude
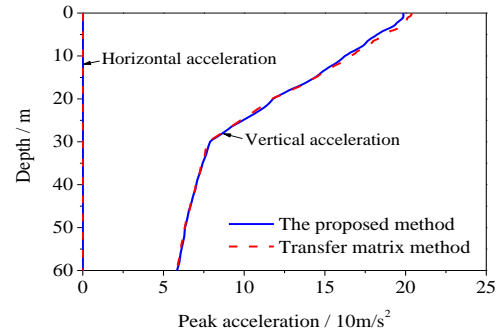

(a) The relative displacement on site surface   (b) The acceleration on site surface

(c) The peak relative displacement along depth   (d) The peak acceleration along depth

(e) The peak maximum principle stress and peak maximum shear stress along depth

Fig. 3 The Leibstadt site responses from the impulse as P wave of 0° angle incidence

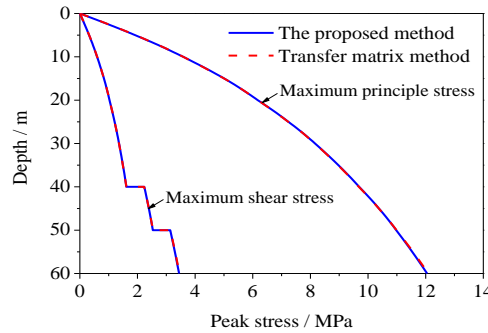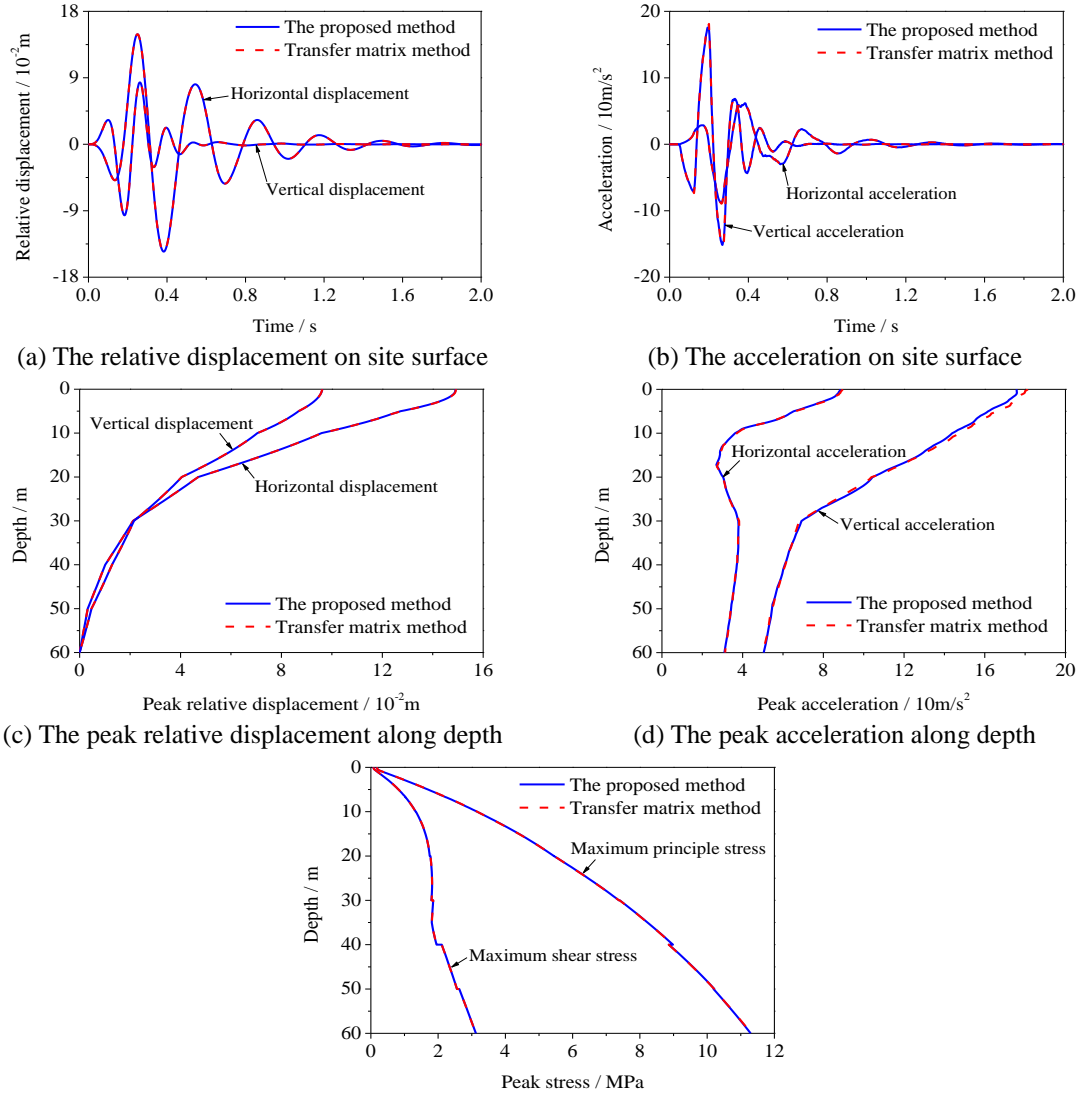(a) The relative displacement on site surface

(b) The acceleration on site surface

(c) The peak relative displacement along depth

(d) The peak acceleration along depth
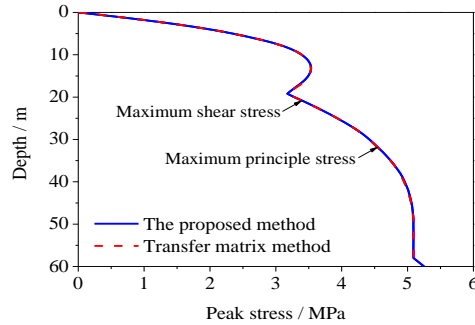
(e) The peak maximum principle stress and peak maximum shear stress along depth

Fig. 4 The Leibstadt site responses from the impulse as P wave of $30°$ angle incidence

$$\mathbf{f} = \left\{ \begin{array}{c} \mathbf{0} \\ \vdots \\ \mathbf{0} \\ (\mathbf{S}+\mathbf{R})\dot{\hat{\mathbf{u}}}^{N-1} \end{array} \right\} \tag{46}$$

The known incident wave velocity vector $\dot{\hat{\mathbf{u}}}^{N-1}$ is given by Eq. (37). The sparse tri-diagonal matrix $\mathbf{C}_B$ comes from the boundary conditions on the free surface, layer interfaces and artificial boundary, and has non-zero values at the corresponding positions. If an interface between the j-th

and (j+1)-th layers is considered, this matrix can be written as

$$
\mathbf{C}_B = \begin{bmatrix} \mathbf{Q}^1 & & & & \\ & \ddots & & & \\ & & \mathbf{Q}^{j+1} - \mathbf{Q}^j & & \\ & & & \ddots & \\ & & & & \mathbf{S} - \mathbf{Q}^{N-1} \end{bmatrix} \tag{47}
$$

Note that the total mass matrix is diagonal. The total stiffness matrix is symmetric five-diagonal. The total damping matrix is non-symmetric seven-diagonal.

For the layer system, it can be easily proved that the dynamic equation Eq. (44) is the time-domain form of the spatial discretization equation in the stiffness matrix method by Kausel and Roesset (1981).

Eq. (44) with the zero initial condition can be solved by the standard time integration algorithm in the structural dynamics, such as the implicit Newmark and Wilson methods. The explicit algorithm proposed by the third author and his coworkers (Du and Wang 2000, Wang *et al.* 2008) can be also used for the efficient computation. The effectiveness of this explicit algorithm to solve the similar dynamic equation also sees the author's work (Zhao *et al.* 2011). The accelerations can be obtained from the displacements and velocities by the dynamic equation.

(a) The relative displacement on site surface

(b) The acceleration on site surface

(c) The peak relative displacement along depth

(d) The peak acceleration along depth

Fig. 5 The Leibstadt site responses from the impulse as SV wave of 0° angle incidence
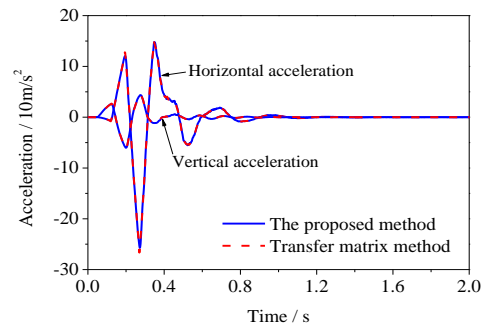
(e) The peak maximum principle stress and peak maximum shear stress along depth
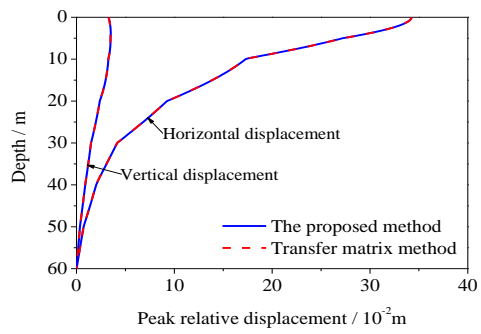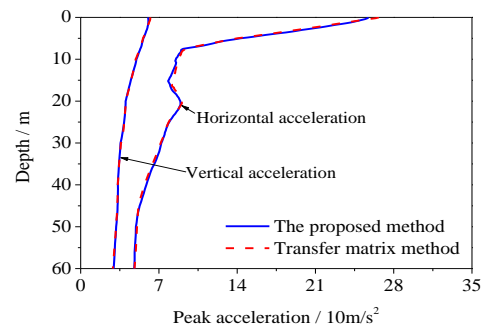
Fig. 5 Continued
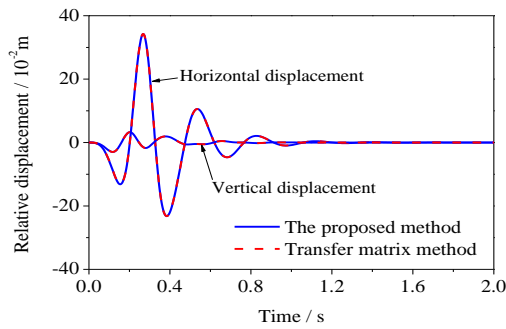
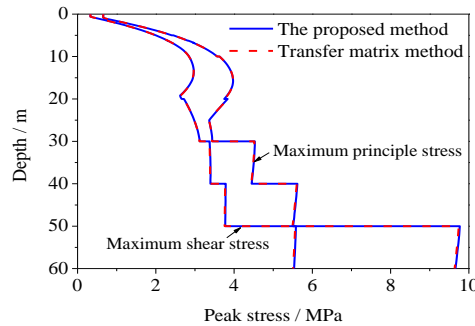(a) The relative displacement on site surface

(b) The acceleration on site surface

(c) The peak relative displacement along depth

(d) The peak acceleration along depth

(e) The peak maximum principle stress and peak maximum shear stress along depth

Fig. 6 The Leibstadt site responses from the impulse as SV wave of 30° angle incidence

4.3 Stress computation

The stress is computed accurately instead of the constant stress element as in the traditional finite element method. First, the nodal forces of an element can be computed by Eq. (39) from the nodal motions. Second, the stresses $\boldsymbol{\sigma}_z^j = \{\tau_{xz}^j \ \sigma_z^j\}^{\mathrm{T}}$ can be obtained by Eq. (32) from the resulting nodal forces. Third, by substituting Eq. (1) into Eq. (3) and then applying Eq. (27) to eliminate the x-derivative of the result, the stress σ_x^j can be obtained as

$$\sigma_x^j = \rho^j \left((c_P^j)^2 - 2(c_S^j)^2\right)\frac{\partial u_z^j}{\partial z} - \frac{\rho^j (c_P^j)^2}{c_x}\dot{u}_x^j \tag{48}$$

where the z-derivative to the displacement is given from the resulting nodal forces. At the layer interfaces, the stresses $\boldsymbol{\sigma}_z^j = \{\tau_{xz}^j \ \sigma_z^j\}^{\mathrm{T}}$ are continuous but the stress σ_x^j does not. The resulting stresses have the same order of accuracy as the displacements.

5. Typical site analysis

The seismic responses of the two typical engineering sites subjected to the obliquely incident plane P or SV wave are calculated by using the proposed 1D finite element artificial boundary method. The two sites are the soft soil and rock sites given in reference (Wolf and Obernhuber 1983). The results obtained by the 1D finite element artificial boundary method are compared with those by the transfer matrix method with fast Fourier transform.

5.1 Soft soil site

The first site is the Leibstadt site in Switzeland (Wolf and Obernhuber 1983). Its geometry and material constants see Table 1. The artificial boundary is set at $z=60$ m so that the responses in a

Table 2 The constants for Koeberg site in South Africa

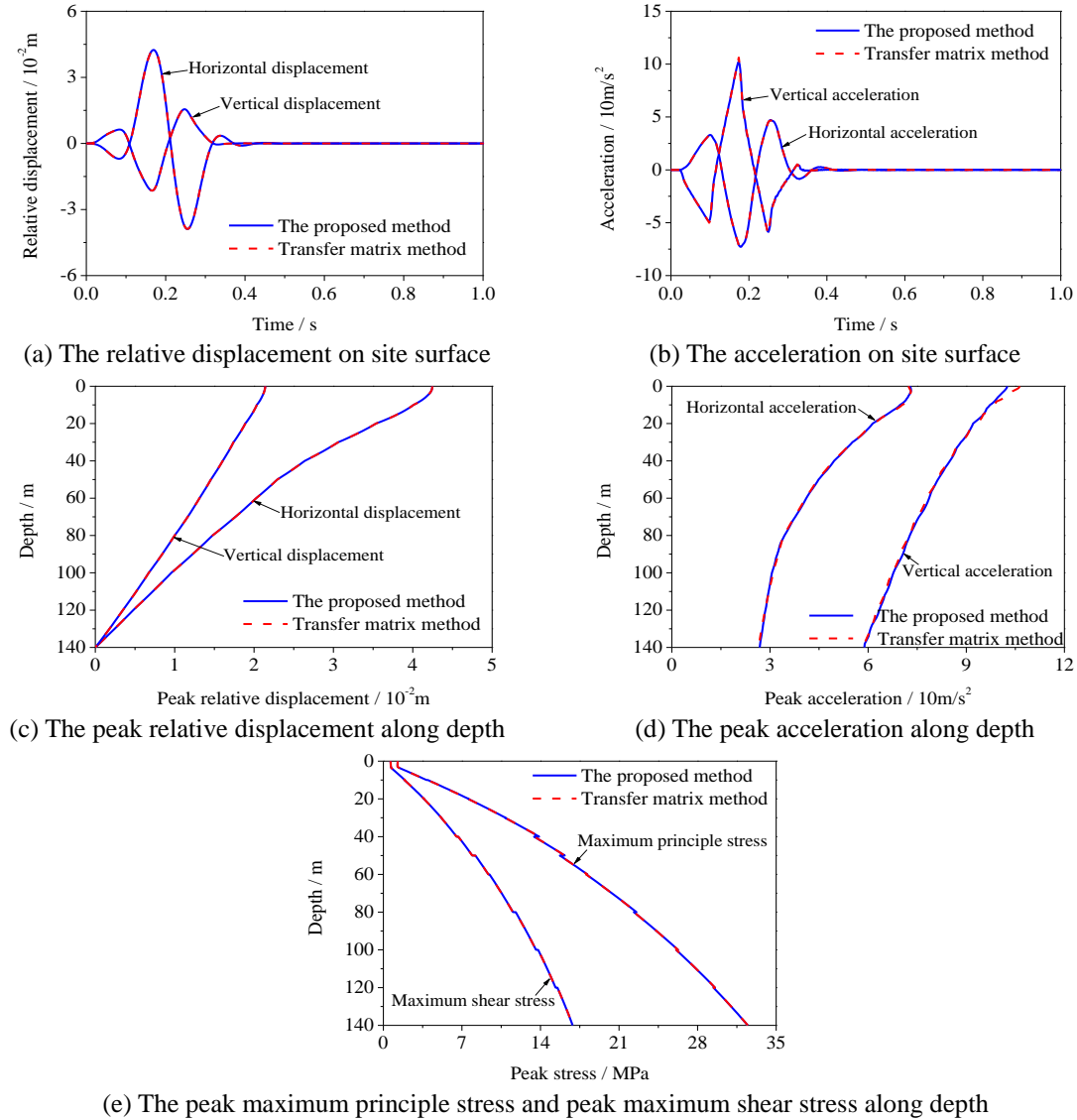| Layer thickness/m	Mass density/kg/m^3	P wave velocity/m/s	S wave velocity/m/s
5	2600	2236	1074
5	2600	2380	1144
10	2600	3397	1387
10	2600	4297	1754
10	2600	5262	2148
10	2600	5477	2631
10	2600	6029	3223
20	2600	6349	3453
20	2600	6856	3848
20	2600	7386	4206
∞	2600	7596	4385
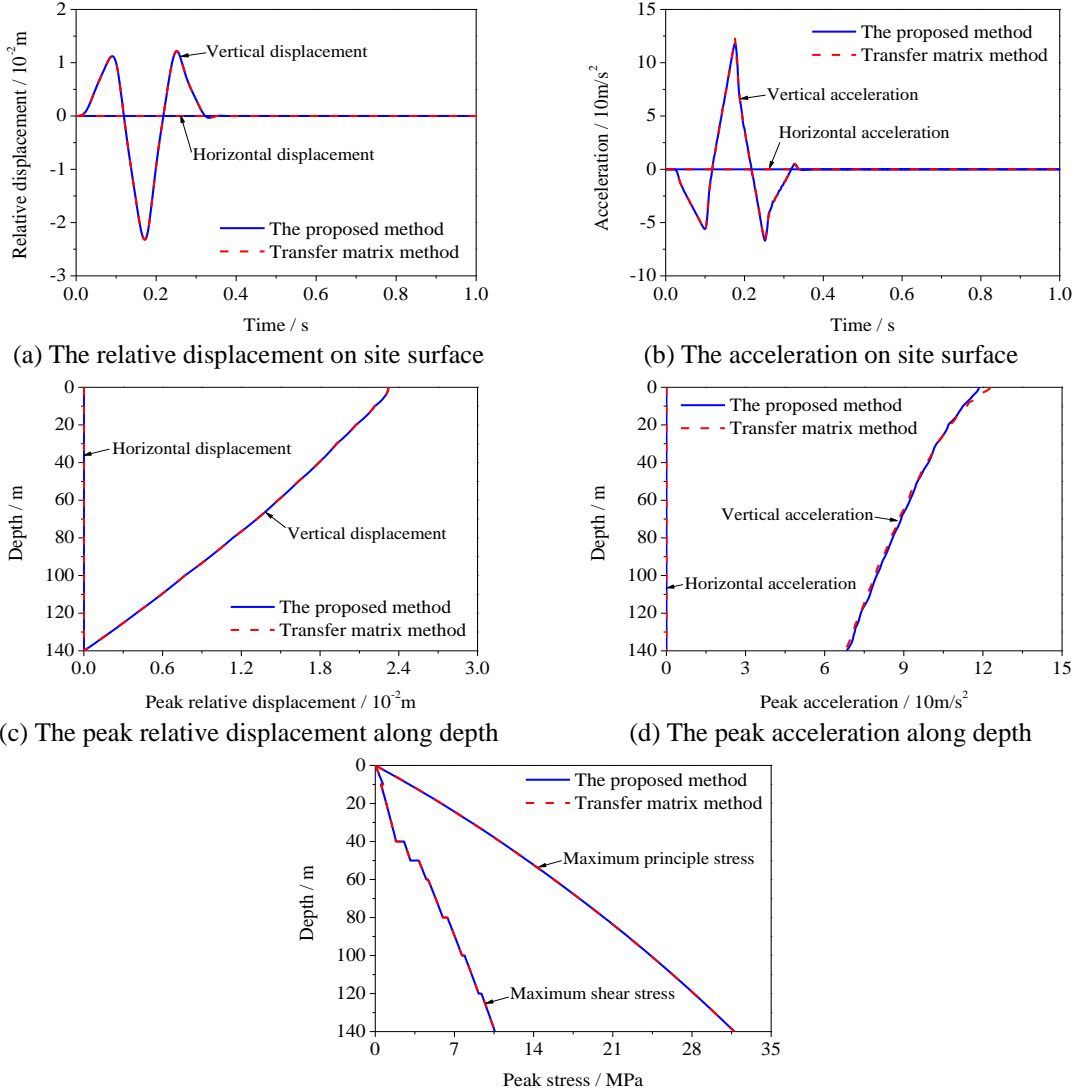
(a) The relative displacement on site surface

(b) The acceleration on site surface

(c) The peak relative displacement along depth

(d) The peak acceleration along depth

(e) The peak maximum principle stress and peak maximum shear stress along depth

Fig. 7 The Koeberg site responses from the impulse as P wave of $0°$ angle incidence

part of underlying half space can be observed. The plane wave is obliquely incident at the artificial boundary. The time history at the intersection point of the artificial boundary and z coordinate axis is chosen as a finite difference approximation of Dirac delta function. The displacement time history can be written as

$$u_0(t) = 16A \left[Z\left(\frac{t}{T}\right) - 4Z\left(\frac{t}{T} - \frac{1}{4}\right) + 6Z\left(\frac{t}{T} - \frac{1}{2}\right) - 4Z\left(\frac{t}{T} - \frac{3}{4}\right) + Z\left(\frac{t}{T} - 1\right) \right] \quad (49)$$

where $Z(a) = a^3 H(a)$ with Heaviside function $H(a)$ ($H(a) = 0$ if $a < 0$ and $H(a) = 1$ if

(a) The relative displacement on site surface

(b) The acceleration on site surface

(c) The peak relative displacement along depth

(d) The peak acceleration along depth

(e) The peak maximum principle stress and peak maximum shear stress along depth

Fig. 8 The Koeberg site responses from the impulse as P wave of 30° angle incidence

$a \geq 0$); A is the peak value of the impulse; and T is the acting time of the impulse. The frequency spectrum of this impulse is known analytically as

$$U_0(\omega) = \frac{1536AT}{(\omega T)^4} \sin^4\left(\frac{\omega T}{8}\right) e^{-i\frac{\omega T}{2}} \tag{50}$$

where ω is the circular frequency and $i = \sqrt{-1}$ is the imaginary unit. $U_0(0) = 0.375AT$. As shown in Fig. 2, we take the peak value A=0.1 m and the acting time T=0.3 s, so that this impulse load can contain the main frequency region of earthquake. If an earthquake record is used as the
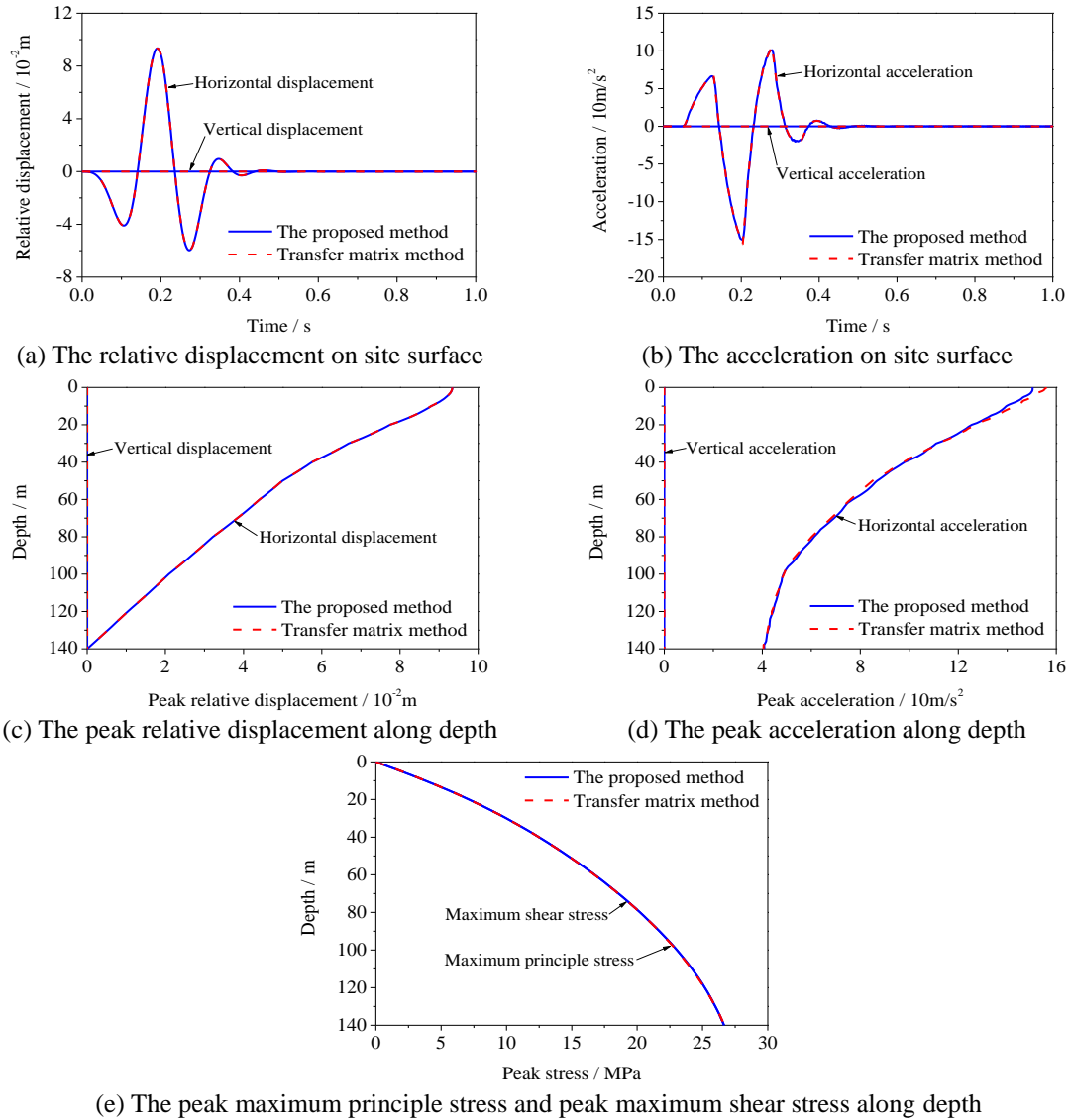
(a) The relative displacement on site surface

(b) The acceleration on site surface

(c) The peak relative displacement along depth

(d) The peak acceleration along depth

(e) The peak maximum principle stress and peak maximum shear stress along depth

Fig. 9 The Koeberg site responses from the impulse as SV wave of 0° angle incidence

incident wave, the displacement results obtained by the transfer matrix method can be identical very well with those by the proposed method. However, the acceleration and stress results contain noises due to the fast Fourier transform. This leads to that the two methods cannot be compared. The impulse is therefore chosen instead of an earthquake record. The proposed method avoids the noises arising from the fast Fourier transform used in the frequency-domain method.

The impulse shown in Fig. 2 is used to form the incident P or SV wave. The finite-element spatial and temporal steps satisfying the requirements of the accuracy and stability are chosen in the 1D finite element artificial boundary method. For the P wave incidence, the proposed method is effective for the incident angle varying from 0° to 90°, and its results are identical very well

(a) The relative displacement on site surface

(b) The acceleration on site surface

(c) The peak relative displacement along depth

(d) The peak acceleration along depth

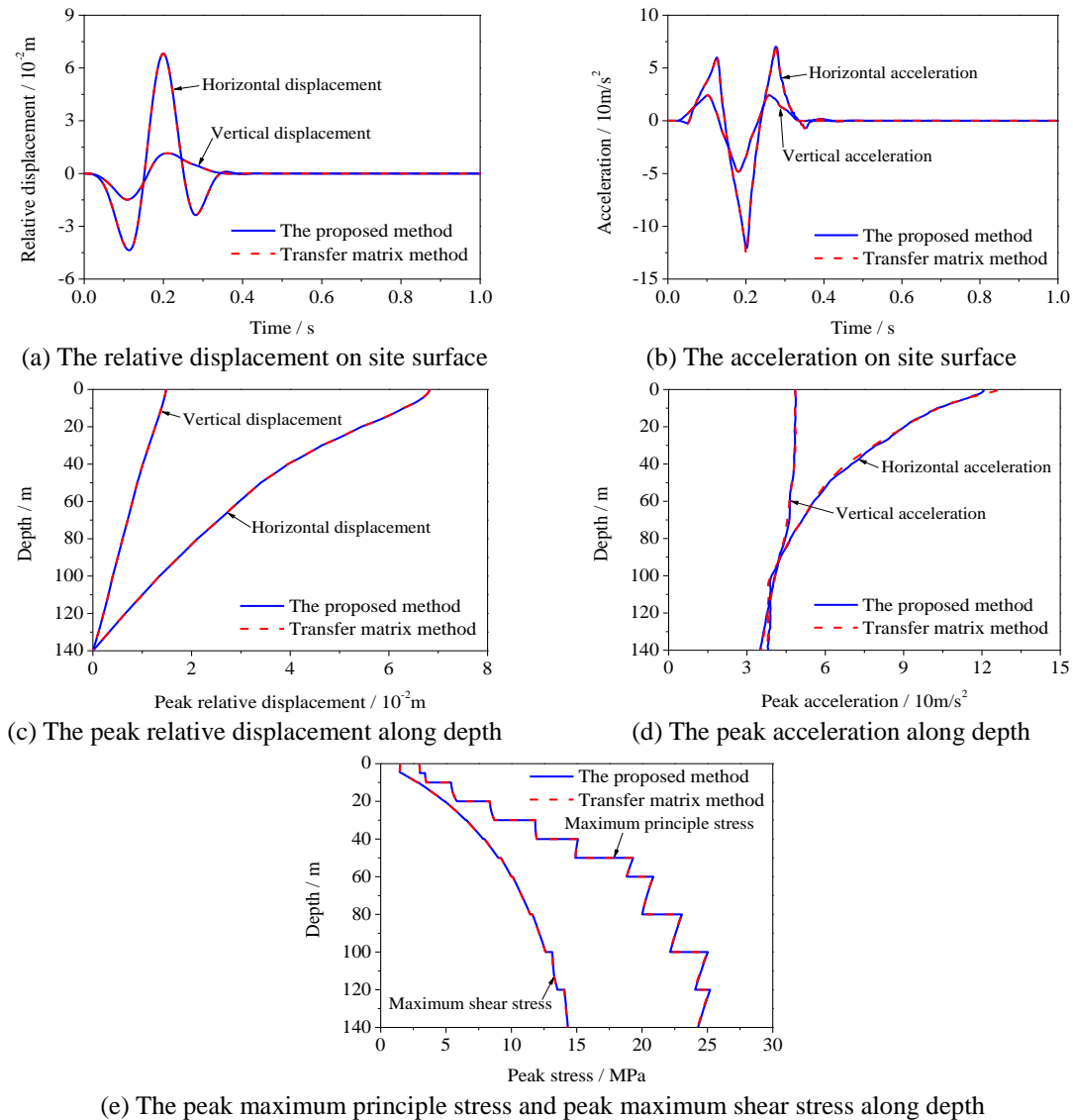(e) The peak maximum principle stress and peak maximum shear stress along depth

Fig. 10 The Koeberg site responses from the impulse as SV wave of 30° angle incidence

with those of the transfer matrix method with fast Fourier transform. Note that the acceleration results are slightly different, which arises from the noises caused by the fast Fourier transform in the transfer matrix method. The results of two typical incident angles 0° and 30° are shown in Figs. 3 and 4, respectively. The results in each figure are (a) the time histories of the horizontal and vertical displacements on the site surface relative to those at the location of impulse incidence, (b) the time histories of the horizontal and vertical accelerations on the site surface, (c) the peak values of the relative horizontal and vertical displacement time histories varying along depth, (d) the peak values of the horizontal and vertical acceleration time histories varying along depth, and (e) the peak values of the maximum principal and maximum shear stress time histories varying along

depth, respectively. It can be noted that the proposed method is applicable to the vertical incidence of $0°$ angle by setting $1/c_x=0$.

For the SV wave incidence, the proposed method is effective for the incident angle varying from $0°$ to the critical angle, and its results are still identical very well with those of the transfer matrix method except the slightly distinguishable acceleration. The SV wave critical angle of this site is about $32.31°$. The results of two typical incident angles $0°$ and $30°$ are shown in Figs. 5 and 6, respectively. In each figure the same subfigures as those in the P wave incidence case are given.

5.2 Rock site

The second site is the Koeberg site in South Africa (Wolf and Obernhuber 1983). Its geometry and material constants see Table 2. The artificial boundary is set at $z=140$ m so that the responses in a part of underlying half space can be observed. The time history shown in Fig. 2 is used to form the plane P or SV wave of incidence at the artificial boundary. The 1D finite element artificial boundary method is effective for this rock site just as for the above soft soil site. The results are still identical very well with those of the transfer matrix method. For the P wave incidence, the results of two typical incident angles $0°$ and $30°$ are shown in Figs. 7 and 8, respectively. For the SV wave incidence, the critical angle of this site is about $35.26°$, and the results of two typical incident angles $0°$ and $30°$ are shown in Figs. 9 and 10, respectively. In each figure the same subfigures as those in the soft soil site are given.

6. Conclusions

The 1D finite element artificial boundary method is proposed to solve the plane wave propagation in the elastic layered half space from the oblique incident seismic wave. The proposed method is compared in detail with the well-known stiffness matrix method proposed by Kausel and Roesset (1981). It is proved that the proposed method is the time-domain form of the spatial discrete revision of the frequency-domain stiffness matrix method for the plane elastic wave propagation case. The proposed method is applied to analyze the Leibstadt site in Switzeland and the Koeberg site in South Africa subjected to the obliquely incident plane body wave. The solutions obtained by the proposed method are identical very well with those by the frequency-domain transfer matrix method with fast Fourier transform. Because the transfer matrix method is the origin of the stiffness matrix method, the above results in the numerical experiments should be obvious in theory. The present paper considers only the homogeneous plane elastic wave propagation in the layered half space. Its extension to the inhomogeneous plane wave case, the soil damping case and the nonlinear soil material case will be studied in the future.

Acknowledgments

References

Barbosa, J.M.O., Park, J. and Kausel, E. (2012), "Perfectly matched layers in the thin layer method", *Comput. Meth. Appl. Mech. Eng.*, **217**, 262-274.

Dunkin, J.W. (1965), "Computation of modal solutions in layered, elastic media at high frequencies", *Bull. Seismol. Soc. Am.*, **55**(2), 335-358.

Du, X. and Wang, J. (2000), "An explicit difference formulation of dynamic response calculation of elastic structure with damping", *Eng. Mech.*, **17**, 37-43. (in Chinese)

Gilbert, F. and Backus, G.E. (1966), "Propagator matrices in elastic wave and vibration problem", *Geophys.*, **31**(2), 326-332.

Haskell, N.A. (1953), "The dispersion of surface waves on multilayered media", *Bull. Seismol. Soc. Am.*, **43**(1), 17-34.

Hashash, Y.M.A., Phillips, C. and Groholski, D.R. (2010), "Recent advances in non-linear site response analysis", *Proceedings of the Fifth International Conference on Recent Advances in Geotechnical Earthquake Engineering and Soil Dynamics*, San Diego, California.

Jones, S. and Hunt, H. (2011), "Effect of inclined soil layers on surface vibration from underground railways using the thin-layer method", *J. Eng. Mech.*, ASCE, **137**(12), 887-900.

Knopoff, L. (1964), "A matrix method for elastic wave problems", *Bull. Seismol. Soc. Am.*, **54**(1), 431-438.

Kausel, E. and Roësset, J.M. (1981), "Stiffness matrices for layered soils", *Bull. Seismol. Soc. Am.*, **71**(6), 1743-1761.

Kausel, E. and Peek, R. (1982), "Dynamic loads in the interior of a layered stratum: an explicit solution", *Bull. Seismol. Soc. Am.*, **72**(5), 1459-1481.

Kausel, E. (1994), "Thin-layer method: formulation in the time domain", *Int. J. Numer. Meth. Eng.*, **37**(6), 927-941.

Kausel, E. (2000), "The Thin-layer method in seismology and earthquake engineering", *Wave Motion in Earthquake Engineering*, WIT Press, UK.

Kausel, E. (2004), "Accurate stresses in the thin-layer method", *Int. J. Numer. Meth. Eng.*, **61**(3), 360-379.

Kausel, E. (2006), *Fundamental Solutions in Elastodynamics*, Cambridge University Press, New York, NY, USA.

Lysmer, J. and Kuhlemeyer, R.L. (1969), "Finite dynamic model for infinite media", *J. Eng. Mech. Div.*, ASCE, **95**(4), 869-877.

Lysmer, J. (1970), "Lumped mass method for Rayleigh waves", *Bull. Seismol. Soc. Am.*, **60**(1), 89-104.

Lysmer, J. and Waas, G. (1972), "Shear waves in plane infinite structures", *J. Eng. Mech. Div.*, ASCE, **18**(1), 85-105.

Liao, H., Chen, Q. and Xu, Z. (1994), "Nonlinear responses of layered soils to obliquely incident SH waves", *J. Tongji Univ.*, **22**(4), 517-522. (in Chinese)

Liu, J. and Wang, Y. (2006), "A 1-D time-domain method for 2-D wave motion in elastic layered half-space by antiplane wave oblique incidence", *Chinese J. Theo. Appl. Mech.*, **38**(2), 219-225. (in Chinese)

Liu, J. and Wang, Y. (2007), "A 1D time-domain method for in-plane wave motions in a layered half-space", *Acta Mechanica Sinica*, **23**(6), 673-680.

Mayoral, J.M., Flores, F.A. and Romo, M.P. (2011), "Seismic response evaluation of an urban overpass", *Earthq. Eng. Struct. Dyn.*, **40**(8), 827-845.

Park, J. and Kausel, E. (2004), "Numerical dispersion in the thin-layer method", *Comput. Struct.*, **82**(7), 607-625.

Rota, M., Lai, C.G. and Strobbia, C.L. (2011), "Stochastic 1D site response analysis at a site in central Italy", *Soil Dyn. Earthq. Eng.*, **31**(4), 626-639.

Seale, S.H. and Kausel, E. (1984), "Dynamic loads in layered halfspaces", *Proceedings of the Fifth Engineering Mechanics Division Specialty Conference*, Laramie, Wyoming.

Seale, S.H. and Kausel, E. (1989), "Point loads in cross-anisotropic layered halfspaces", *J. Eng. Mech.*, ASCE, **115**(3), 509-542.

Thomson, W.T. (1950), "Transmission of elastic waves through a stratified solid medium", *J. Appl. Phys.*, **21**(1), 89-93.

Takano, S., Yasui, Y., Takeda, T. and Miyamoto, A. (1988), "The new method to calculate the response of layered half-space subjected to obliquely incident body wave", *Proceedings of the Ninth World Conference on Earthquake Engineering*, Tokyo-Kyoto, Japan.

Watson, T.H. (1970), "A note on fast computation of Rayleigh wave dispersion in the multilayered elastic half-space", *Bull. Seismol. Soc. Am.*, **60**(1), 161-166.

Wolf, J.P. and Obernhuber, P. (1982), "Free-field response from inclined SH-waves and Love-waves", *Earthq. Eng. Struct. Dyn.*, **10**(6), 823-845.

Wolf, J.P. and Obernhuber, P. (1982), "Free-field response from inclined SV- and P-waves and Rayleigh-waves", *Earthq. Eng. Struct. Dyn.*, **10**(6), 847-869.

Wolf, J.P. and Obernhuber, P. (1983), "In-plane free-field response of actual sites", *Earthq. Eng. Struct. Dyn.*, **11**(1), 121-134.

Wolf, J.P. (1985), *Dynamic Soil-Structures Interaction*, Prentice-Hall.

Wang, J., Zhang, C. and Du X. (2008), "An explicit integration scheme for solving dynamic problems of solid and porous media", *J. Earthq. Eng.*, **12**(2), 293-311.

Zhao, M., Du, X., Liu, J. and Liu, H. (2011), "Explicit finite element artificial boundary scheme for transient scalar waves in two-dimensional unbounded waveguide", *Int. J. Numer. Meth. Eng.*, **87**(11), 1074-1104.

CC